Nuclear Engineering and Technology 52 (2020) 878–888

Contents lists available at ScienceDirect

Nuclear Engineering and Technology

journal homepage: www.elsevier.com/locate/net

Original Article

Validation of UNIST Monte Carlo code MCS using VERA progression problems

Tung Dong Cao Nguyen, Hyunsuk Lee, Sooyoung Choi, Deokjung Lee*

Department of Nuclear Engineering, Ulsan National Institute of Science and Technology (UNIST), 50 UNIST-gil, Ulsan, 44919, Republic of Korea

ARTICLE INFO

Article history:
Received 18 June 2019
Received in revised form
24 September 2019
Accepted 29 October 2019
Available online 1 November 2019

Keywords:
Monte Carlo
Core simulation
Zero power physics test
Validation
MCS

ABSTRACT

This paper presents the validation of UNIST in-house Monte Carlo code MCS used for the high-fidelity simulation of commercial pressurized water reactors (PWRs). Its focus is on the accurate, spatially detailed neutronic analyses of startup physics tests for the initial core of the Watts Bar Nuclear 1 reactor, which is a vital step in evaluating core phenomena in an operating nuclear power reactor. The MCS solutions for the Consortium for Advanced Simulation of Light Water Reactors (CASL) Virtual Environment for Reactor Applications (VERA) core physics benchmark progression problems 1 to 5 were verified with KENO-VI and Serpent 2 solutions for geometries ranging from a single-pin cell to a full core. MCS was also validated by comparing with results of reactor zero-power physics tests in a full-core simulation. MCS exhibits an excellent consistency against the measured data with a bias of ±3 pcm at the initial criticality whole-core problem. Furthermore, MCS solutions for rod worth are consistent with measured data, and reasonable agreement is obtained for the isothermal temperature coefficient and soluble boron worth. This favorable comparison with measured parameters exhibited by MCS continues to broaden its validation basis. These results provide confidence in MCS's capability in high-fidelity calculations for practical PWR cores.

1. Introduction

The Consortium for Advanced Simulation of Light Water Reactors (CASL) [1] provided detailed specifications for the VERA core physics benchmark progression [2] in 2014, including 10 problems based on the actual fuel and plant data of the Watts Bar Nuclear Plant Unit 1 (WBN1) initial startup core. This information provides technical assistance to nuclear industry software, method developers, and researchers with an enhanced modeling and simulation (M&S) package of both single and coupled reactor physics/thermal-hydraulics problems. In these problems, the analysis of neutronic performance is key for detecting the phenomena of an operating nuclear power reactor. To achieve accurate, spatially detailed core eigenvalue and power distribution prediction capabilities for large-scale nuclear reactors, the Monte Carlo (MC) reactor physics analysis tool has become increasingly common; the MC method is helpful in solving complex three-dimensional (3D) problems and is especially suitable for complex geometries that cannot be explicitly simulated using deterministic methods. However, it requires much longer computation times than the deterministic method to achieve a small statistical uncertainty. Fortunately, the extensive development of computer science and technology permits the application of the MC method in reactor core simulations and analyses. Labossiere-Hickman et al. recently researched selected VERA core physics benchmarks for an individual fuel assembly and a whole core under beginning-of-cycle and hot zero-power conditions; using WBN1 data, the MC code OpenMC was compared with the deterministic code system VERA-CS [3]. A more detailed analysis was performed by Luo et al. by employing the MC code RMC developed at Tsinghua University [4].

To promote an advanced neutron-physics M&S, the Ulsan National Institute of Science and Technology (UNIST) has been developing a MC code named MCS [5–8] to achieve a high-accuracy whole-core solution. Various verification and validation (V&V) studies have been conducted on MCS to ensure its accuracy and reliability for nuclear power system design and safety evaluation [7–16]. Therefore, the primary goal of this work is to verify and validate MCS using several VERA core

* Corresponding author.
E-mail addresses: tungnguyen@unist.ac.kr (T.D.C. Nguyen), hyunsuklee@unist.ac.kr (H. Lee), schoi@unist.ac.kr (S. Choi), deokjung@unist.ac.kr (D. Lee).

https://doi.org/10.1016/j.net.2019.10.023

physics benchmark problems that range from a single-pin cell to a whole-core simulation. This paper is organized as follows. Section 2 introduces and describes the WBN1. Section 3 introduces the UNIST Monte Carlo code MCS and briefly presents the computer codes used as references. Section 4 indicates the neutronic performances, including numerical solutions to the VERA core benchmark problems 1 to 5. Finally, the conclusions and future perspectives are described in Section 5.

2. Watts Bar Nuclear Plant Unit 1

WBN1 is a Westinghouse pressurized water reactor (PWR) operated by the Tennessee Valley Authority (TVA) and is currently operating in its 13th cycle, having logged more than 6000 effective full power days (EFPDs) of operation since 1996 [17]. The initial thermal power was 3411 MW but was uprated by 1.4% in 2001. Fig. 1 shows the quarter-core loading pattern and rod cluster control assembly (RCCA) configurations of WBN1 [2]. Only control bank D is slightly inserted into the core during its operation. This initial loading pattern consists of 3 enrichment zones (with 2.11, 2.62 and 3.10% ^{235}U) with the insertion of several Pyrex burnable absorber cluster assemblies. In addition, 57 RCCAs are grouped into 8 separate banks as shown in Fig. 1. Various core parameters for WBN1 are summarized in Table 1. The reactor core has 193 17 × 17 fuel assemblies with a fuel stack height of 365.76 cm, each with 264 fuel rods and 25 guide or instrumentation tubes. Fig. 2 is a typical radial and axial layout of a fuel assembly, which includes upper and lower core plates, nozzles, gaps, and 2 Inconel and 6 Zircaloy spacer grids [2]. The main parameters for an assembly are summarized in Table 2. See Ref. [2] for full details on WBN1.

Table 1
Main core description for WBN1.

Parameter	Value
No. of assembly	193
Assembly pitch, cm	21.5
Coolant inlet temperature, K	565.0
Inlet coolant density, g/cm3	0.743
Initial boron concentration, ppm	1285
Initial critical Bank D withdraw position, step	167

3. Computer codes

In this study, three MC codes were employed, one for calculation - UNIST MC code MCS, and the other two — KENO-VI and Serpent 2 - as references.

The first code is the UNIST in-house MC code named MCS. It is a 3D continuous-energy neutron physics code for particle transport based on the Monte Carlo method, and has been under development at UNIST since 2013 [[5]][[6]]. Two kinds of calculations are allowed by MCS: criticality runs for reactivity calculations, and fixed-source runs for shielding problems. The neutron transport capability of MCS is verified and validated with many benchmark problems including BEAVRS benchmarks, the International Criticality Safety Benchmark Experimental Problem (ICSBEP) - including 279 validation representative cases of PWR spent fuel pools and storage casks, and the Jordan Research and Training Reactor (JRTR). MCS is capable of whole-core simulation with pin-wise depletion and an internal thermal-hydraulic feedback module; in addition, it is validated against the solution of BEAVRS Cycle 1 [7] [8].

The KENO-VI 3D MC criticality computer code is one of the primary criticality safety analysis tools in SCALE (Standardized Computer Analysis for Licensing Evaluation) [18]. Developed and maintained by the Oak Ridge National Laboratory (ORNL), this code system is widely used by the Nuclear Regulatory Commission (NRC) of the United States to enable standardized analyses and evaluation of nuclear facilities.

The Serpent MC code [19] is a continuous-energy MC reactor physics burnup code with recent applications in radiation shielding, multi-physics, and fusion neutronics. It is currently employed for reactor physics applications, including homogenized group constant generation, burnup calculations, the modeling of small research reactor cores, and multi-physics calculations. Serpent has been developed at the VTT Technical Research Centre of Finland since 2004 and the current development version, Serpent 2, has notably diversified the applications of the code.

4. Numerical results

MCS uses the ENDF/B-VII.0 and ENDF/B-VII.1 continuous cross-section libraries. The MCS simulations were executed on a Linux cluster (Intel Xeon E5-2620 @ 3.00 GHz). Solutions computed by KENO-VI for VERA benchmark problems were obtained from the benchmark document and used as the references for validation. Serpent 2 results were also generated for comparison with exactly same input parameters and cross sections with MCS since, for KENO-VI, only results are available from the CASL report [2] but not the inputs. A few simple problems were conducted by Serpent 2 for the sake of demonstration of the accuracy of MCS. For complex problems, measured data and KENO-VI results are used for the validation of

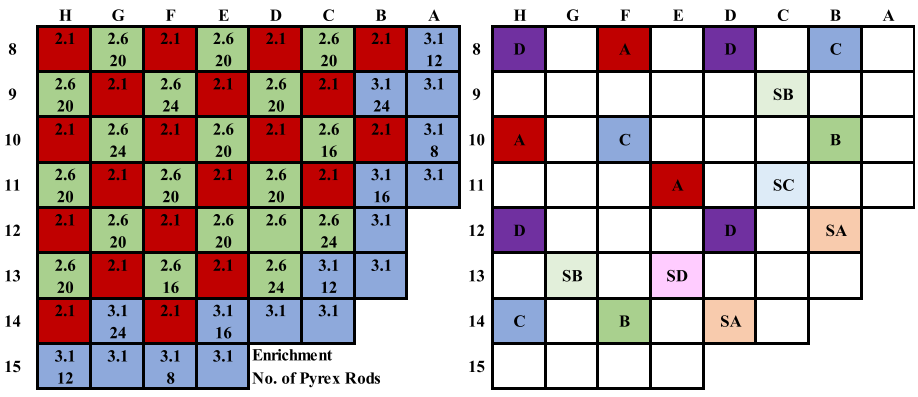

Fig. 1. Assembly, poison, and RCCA configurations for WBN1 (in quarter symmetry) [2].

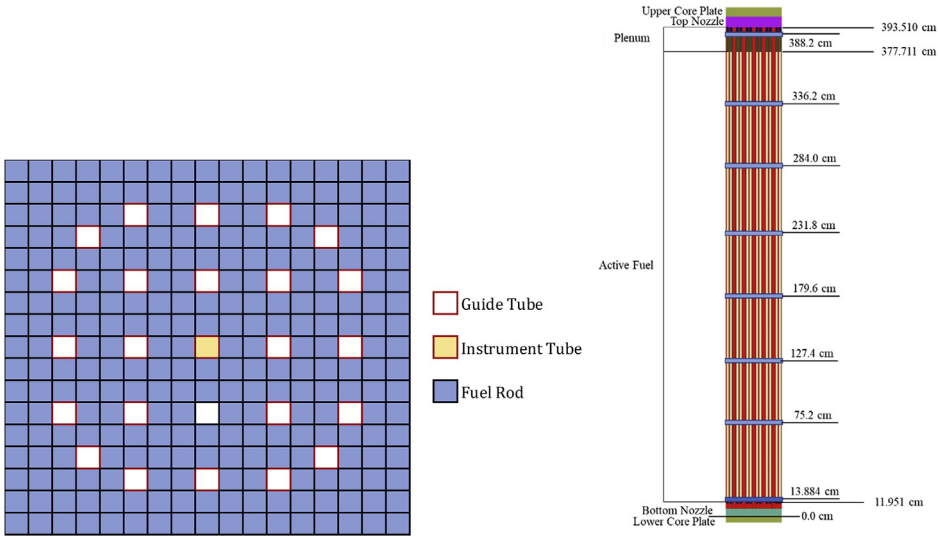

Fig. 2. Fuel assembly radial and axial geometries [2].

Table 2
Assembly description for WBN1.

Parameter	Value
Rod pitch, cm	1.26
Fuel rod height, cm	385.1
Inner-assembly half gap, cm	0.04
Square lattice	17 × 17
No. of fuel rods	264

MCS. The simulations performed with MCS for the VERA startup core layout are listed below. All simulations were performed under hot zero-power (HZP) and beginning-of-cycle (BOC) conditions, except for a few simulations performed at different fuel temperatures.

- Problem 1: 2D HZP BOC pin cell;
- Problem 2: 2D HZP BOC lattice;
- Problem 3: 3D HZP BOC assembly;
- Problem 4: 3D HZP BOC 3 × 3 assembly control rod worth;
- Problem 5: physical reactor zero-power physics tests (ZPPTs).

For all problems 1 to 5, the eigenvalue (k_{eff}) difference is calculated as in Eq. (1), and the relative difference defined in Eq. (2) is employed to compare the power profiles and control rod worth.

$$k_{eff} \text{ difference } [\text{pcm}] = \left(k_{eff,S} - k_{eff,R}\right) \times 10^5, \tag{1}$$

$$\text{Relative difference } [\%] = \frac{S-R}{R} \times 100, \tag{2}$$

where S is the simulated solution by MCS, R is the reference solution, including KENO-VI, Serpent 2 and measured data. The standard deviation of these differences is computed using the error propagation method. It is noted that MCS's deviation is main contributor due to the low KENO-VI's deviation (less than 1pcm for k_{eff} and less than 0.5% for power profiles). In case of the 3D problems, the normalized radial power distribution, which is to be shown below, is averaged over the axial meshes of the active core.

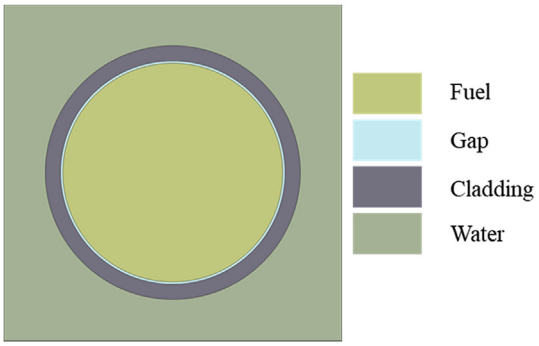

Fig. 3. Problem 1: Pin cell geometry.

4.1. VERA core physics benchmark problem 1

The first VERA core physics benchmark problem demonstrated MCS's capability against an eigenvalue problem for a simple 2D pin cell (shown in Fig. 3). Typical materials for this pin cell are UO_2, Zircaloy-4, water containing soluble boron, and helium gas for the pellet-clad gap. This problem is divided into five calculations. The first four calculations (1A-1D) represent a standard pin cell at BOC conditions with a range of fuel temperatures from 600 to 1200 K that are common under zero- and full-power operating conditions. Problem 1E is an integral fuel burnable absorber (IFBA) fuel rod containing a thin ZrB_2 coating on the UO_2 fuel pellet. The histories for the MC calculations and their average execution times are summarized in Table 3. The eigenvalues (k_{eff}) for the five calculations by MCS, KENO-VI, and Serpent 2 are listed in Table 4. MCS's eigenvalues are in better agreement with those of Serpent 2 (difference within 22 pcm)

Table 3
Problem 1: Average execution time of each code.

Code	Library	Histories	# processes	Execution time (min)
MCS	ENDF/B-VII.0 ENDF/B-VII.1	7.50E+07	8	50
KENO-VI	ENDF/B-VII.0	1.10E+08	192	22
Serpent 2	ENDF/B-VII.0	7.50E+07	12	20

Table 4
Problem 1: k_{eff} by MCS, KENO-VI, and Serpent 2 (at one standard deviation).

No.	Integral Absorber	T_m(K)	T_f(K)	ρ_{mod}(g/cm^3)	MCS			
					k_{eff} (±9 pcm)	Difference with KENO-VI (±12 pcm)	Difference with Serpent 2 (±12 pcm)	Difference with VII.1 (±13 pcm)
1A	None	565	565	0.743	1.18713	9	−11	4
1B	None	600	600	0.661	1.18183	−32	−10	22
1C	None	600	900	0.661	1.17171	−1	3	14
1D	None	600	1200	0.661	1.16326	66	15	28
1E	IFBA	600	600	0.743	0.77110	−59	−22	−23

Table 5
Problem 2: Average execution time of each code.

Code	Library	Histories	# processes	Execution time (min)
MCS	ENDF/B-VII.0	1.05E+08	36	22
KENO-VI	ENDF/B-VII.0	1.10E+09	300	180
Serpent 2	ENDF/B-VII.0	1.05E+08	28	15

than with those of KENO-VI (difference of up to 66 pcm), when Serpent 2 models and input setting options are the same as those of MCS. Additional calculations by MCS obtained with the ENDF/B-VII.1 library show that the differences between the ENDF/B-VII.0 and ENDF/B-VII.1 neutron libraries for a simple pin cell problem are within 28 pcm.

4.2. VERA core physics benchmark problem 2

The second VERA core physics benchmark problem demonstrated MCS's performances in modeling a simple 2D fuel lattice located at the central axial region of PWR fuel assemblies. This problem is a single Westinghouse 17 × 17-type fuel lattice at BOC as shown in Fig. 2; the assembly geometry parameters were provided in Section 2. The neutron poisons inserted into the guide tubes are silver-indium-cadmium (AIC), boron carbide (B_4C), Pyrex (borosilicate glass: B_2O_3–SiO_2), and B_4C–Al_2O_3. The instrument tube thimble and other structural materials are made of 304 stainless steel. An IFBA and gadolinia are also included in some of the test cases as integral burnable absorbers. This problem is divided into many calculations. The first (2A) introduces a typical zero-power fuel lattice under isothermal conditions. Other calculations (2B–2D) are for the same geometry, but with fuel temperatures ranging from 600 to 1200 K. Calculations 2E to 2P analyze the capability to accurately simulate radially heterogeneous features such as different burnable poisons and control rod types. Finally, 2Q tests a code's capability to accurately simulate the reactivity depression by a spacer grid. Table 5 lists the average execution times of MCS, KENO-VI, and Serpent 2 for each calculation. The summary of MCS eigenvalues and comparisons with KENO-VI and Serpent 2 for each Problem 2 case are provided in Table 6. Again, results indicate that MCS solutions are more consistent with those of Serpent 2 (less than 15 pcm in k_{eff} difference) than with those of KENO-VI.

4.3. VERA core physics benchmark problem 3

This core physics benchmark problem demonstrated MCS's performance for a simple 3D fuel assembly. It consists of a single Westinghouse 17 × 17-type fuel assembly under BOC and HZP isothermal conditions, as described in Section 2 except that the assembly is 3D rather than 2D. The problem is divided into two calculations, 3A and 3B. Table 7 indicates the average execution times of MCS, KENO-VI, and Serpent 2 for each calculation. As shown in Table 8, MCS predicts an eigenvalue approximately 30 pcm lower than that of KENO-VI. However, the k_{eff} of MCS is more consistent with that of Serpent 2, with differences within 11 pcm. The MCS power profiles for each case are compared with those of KENO-VI in Figs. 4 and 5. The maximum relative standard deviations (SD) of the MCS radial and axial power profiles are 0.16% and 1.97%, respectively. As the majority of KENO-VI's relative SD values are less than 0.01%, the MCS SD is the main contributor to the SD of the differences in power profiles. In general, power profiles are in excellent agreement: the root-mean-square (RMS) difference in radial power profiles is less than 0.5%, and the maximum relative

Table 6
Problem 2: k_{eff} by MCS, KENO-VI, and Serpent 2 (at one standard deviation).

No.	Description	T_f(K)	ρ_{mod} (g/cm^3)	MCS		
				k_{eff} (±7 pcm)	Difference with KENO-VI (±9 pcm)	Difference with Serpent 2 (±9 pcm)
2A	No Poisons	565	0.743	1.18244	26	−6
2B	No Poisons	600	0.661	1.18299	−37	−13
2C	No Poisons	900	0.661	1.17401	26	14
2D	No Poisons	1200	0.661	1.16588	29	−15
2E	12 Pyrex	600	0.743	1.06924	−39	15
2F	24 Pyrex	600	0.743	0.97539	−63	−4
2G	24 AIC	600	0.743	0.84688	−81	−2
2H	24 B4C	600	0.743	0.78726	−96	3
2I	Instrument Thimble	600	0.743	1.17953	−39	−13
2J	Instrument + 24 Pyrex	600	0.743	0.97463	−56	−4
2K	Zoned + 24 Pyrex	600	0.743	1.01947	−59	−8
2L	80 IFBA	600	0.743	1.01854	−38	4
2 M	128 IFBA	600	0.743	0.93834	−45	−3
2 N	104 IFBA + 20 WABA	600	0.743	0.86913	−49	7
2O	12 Gadolinia	600	0.743	1.04733	−40	10
2P	24 Gadolinia	600	0.743	0.92698	−43	−11
2Q	Zircaloy Spacer Grid	565	0.743	1.17228	34	13

Table 7
Problem 3: Average execution time of each code.

Code	Library	Histories	# processes	Execution time (min)
MCS	ENDF/B-VII.0	1.05E+08	24	150
KENO-VI	ENDF/B-VII.0	2.50E+10	240	7200
Serpent 2	ENDF/B-VII.0	1.05E+08	12	45

difference in axial power profiles is less than 2.0% (with most differences within 1.0%).

4.4. VERA core physics benchmark problem 4

This problem is based on the 3D assembly problem with the addition of multiple assemblies and RCCAs as shown in Fig. 6. Its

Table 8
Problem 3: k_{eff} by MCS, KENO-VI, and Serpent 2 (at one standard deviation).

No.	Description	Enrichment (%)	Boron (ppm)	Temp. (K)	MCS		
					k_{eff} (±7 pcm)	Difference with KENO-VI (±8 pcm)	Difference with Serpent 2 (±8 pcm)
3A	No Poisons	3.100	1300	600	1.17547	−25	3
3B	16 Pyrex	2.619	1066	565	0.99982	−33	11

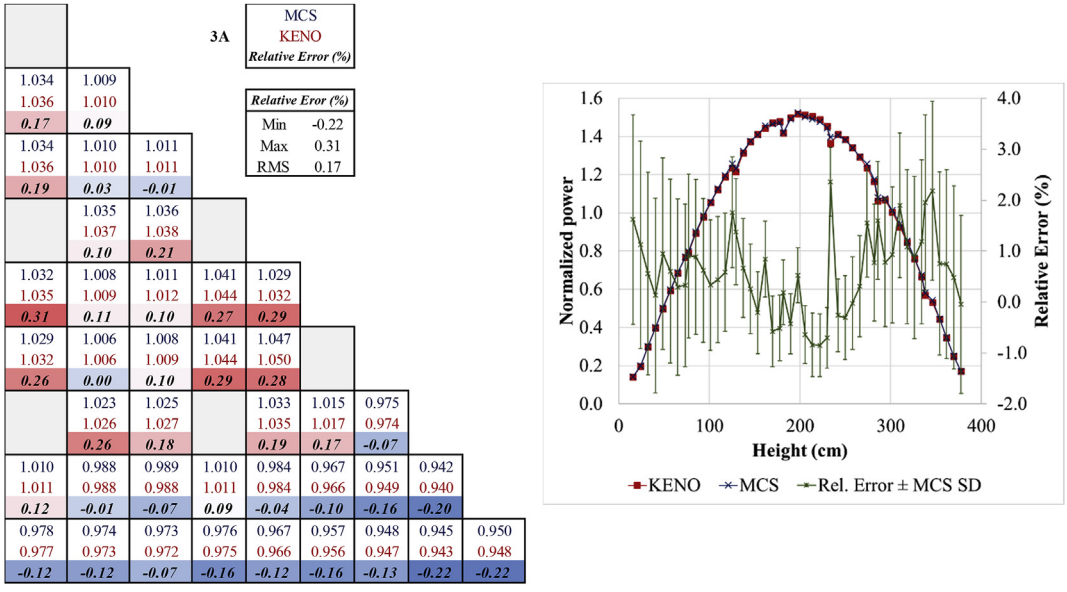

Fig. 4. Problem 3A: Radial (left) and axial (right) power profiles.

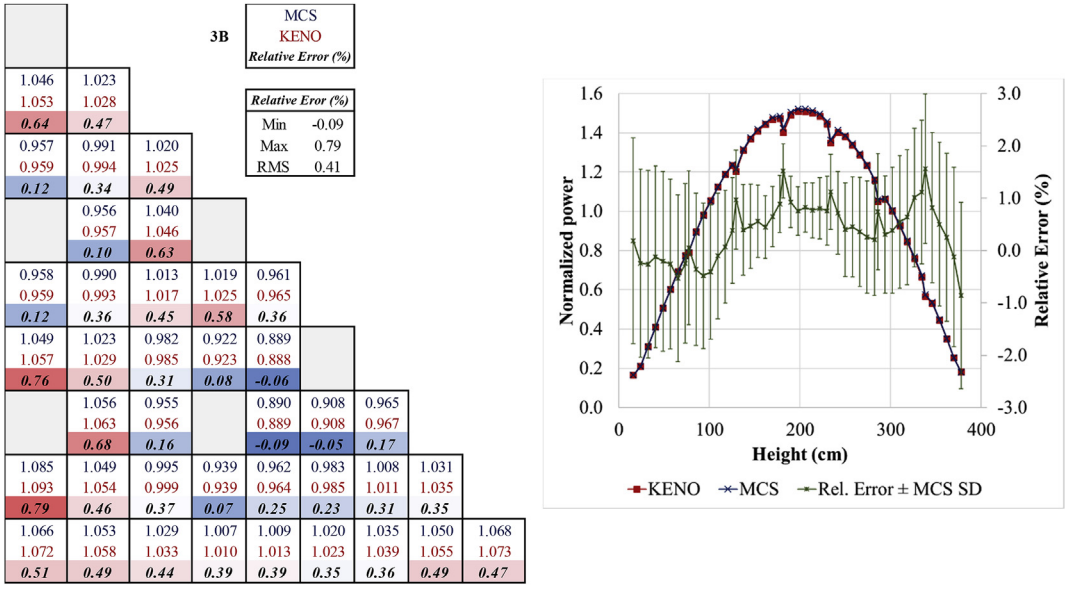

Fig. 5. Problem 3B: Radial (left) and axial (right) power profiles.

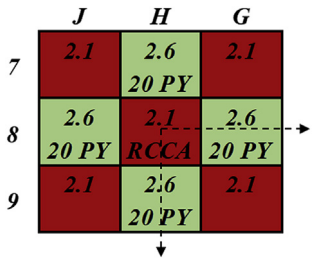

Fig. 6. Problem 4: Assembly, poison, and control layout [2].

Table 9
Problem 4: Average execution time of each code.

Code	Library	Histories	# processes	Execution time (min)
MCS	ENDF/B-VII.0	1.05E+08	24	154
KENO-VI	ENDF/B-VII.0	5.00E+09	300	1560

DRW and IRW discrepancies are 5.8% and 2.4%, respectively. The corresponding RCCA DRW and IRW are also compared in Fig. 9. The normalized radial and axial power profiles are shown in Figs. 10–12. Owing to a large number of particle histories, the radial and axial power uncertainties of the MCS code are respectively less than 0.6% and 3.2% (at the top of the assembly). Again, those MCS uncertainties are the main contributors to the SD of the differences in power profiles between MCS and KENO-VI because of the small relative SD of the KENO-VI power. The power profiles of MCS also show good agreement with those of KENO-VI: the relative differences are less than 0.05% for the radial distribution and 1.5% for most of the axial distributions (with a maximum of approximately 4% at the top of the assembly where the power is small owing to the RCCA insertion).

4.5. VERA core physics benchmark problem 5

The geometry for problem 5 consists of a whole core of Westinghouse 17 × 17-type fuel assemblies in the WBN1 initial loading pattern. The solutions by MCS are for the zero-power physics tests (ZPPT) and core power profiles under a zero-power condition without thermal-hydraulic feedback and depletion. A total of 300 million histories were run with 10 inactive batches, 40 active batches, and 6,000,000 histories per batch (300 cycles per batch) for the eigenvalue search. Both MCS and KENO-VI used the ENDF/B-VII.0 cross-section library for this problem. Table 12 indicates the average execution times of MCS and KENO-VI for each eigenvalue search, and Table 13 summarizes the MCS numerical results for the initial criticality configuration in which control bank D is partially inserted into the core. Other RCCA banks are also inserted. The average difference in eigenvalues between MCS and KENO-VI is 26 pcm. In addition, the ZPPT series includes the DRW of each RCCA bank, the differential boron worth (DBW), and the isothermal temperature coefficient (ITC), which are commonly used for the validation and verification of nuclear numerical methods. Solutions obtained by MCS were compared with the measured data [2] and KENO-VI results and are summarized in Table 14. MCS solutions are clearly consistent with the measured data and KENO-VI results, as the largest differences in the rod worth are 6.0% and 7.9%, respectively. Reasonable agreement on ITC and soluble boron worth is

Table 10
Problem 4: k_{eff} for 2D 3 × 3 lattice (at one standard deviation).

Case	Description	MCS		Difference vs. KENO-VI	
		k_{eff} [±3 pcm]	Rod worth [±4 pcm]	k_{eff} [±3 pcm]	Rod worth [%]
4A-2D	**Uncontrolled**	1.00994	–	−30	–
4B-2D	AIC controlled	0.98312	2701	−33	0.17 ± 0.15
4C-2D	**B_4C controlled**	0.97983	3043	−46	0.61 ± 0.13

solutions show the ability to predict the eigenvalue (k_{eff}) and power distribution without the thermal-hydraulic feedback or the depletion in the presence of black neutron absorbers. The control rod reactivity worth, related to the movement of the RCCAs, is commonly used for the verification of nuclear numerical methods. The differential rod worth (DRW) and integral rod worth (IRW) were also obtained by MCS and compared with the reference results. Table 9 indicates the average execution times of MCS and KENO-VI for each eigenvalue calculation. First, the 2D calculations were conducted with uncontrolled and controlled cases. Table 10 summarizes the k_{eff} by MCS and KENO-VI for each case. MCS underestimates k_{eff} by approximately 37 pcm and predicts the rod worth with a difference less than 18 pcm compared with KENO-VI. The assembly-wise and pin-wise power profiles were also obtained by MCS and compared with those of KENO-VI, as shown in Figs. 7 and 8. The comparison shows that the RMS difference in assembly power is less than 0.2% and the maximum difference in pin power is less than 1.5% for all cases. Second, the MCS numerical results for the 3D case are compared with KENO-VI results in Table 11. MCS solutions are clearly consistent with KENO-VI reference results, as the largest difference in k_{eff} is 34 pcm. In addition, the maximum

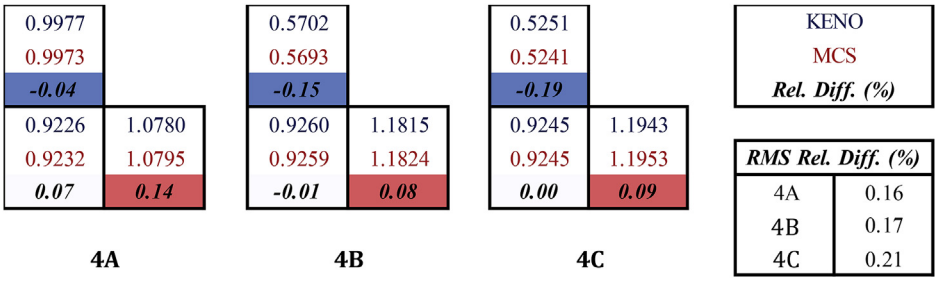

Fig. 7. Problem 4-2D: Assembly power distribution.

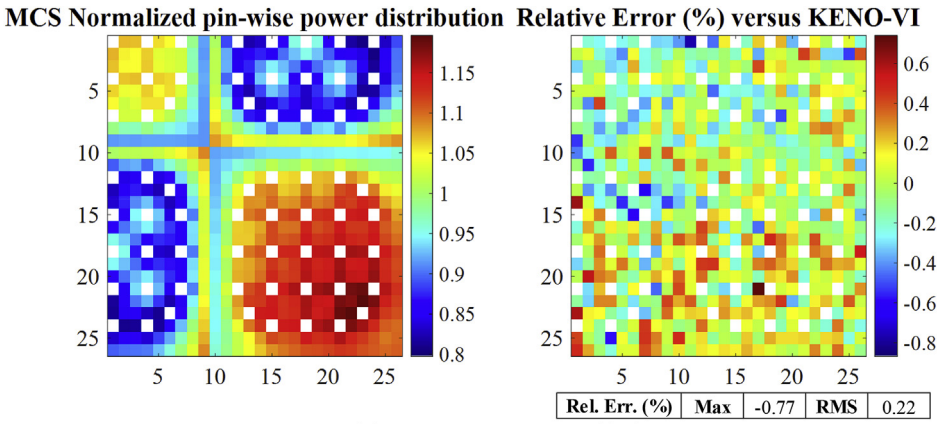

(a) 4A-2D: uncontrolled

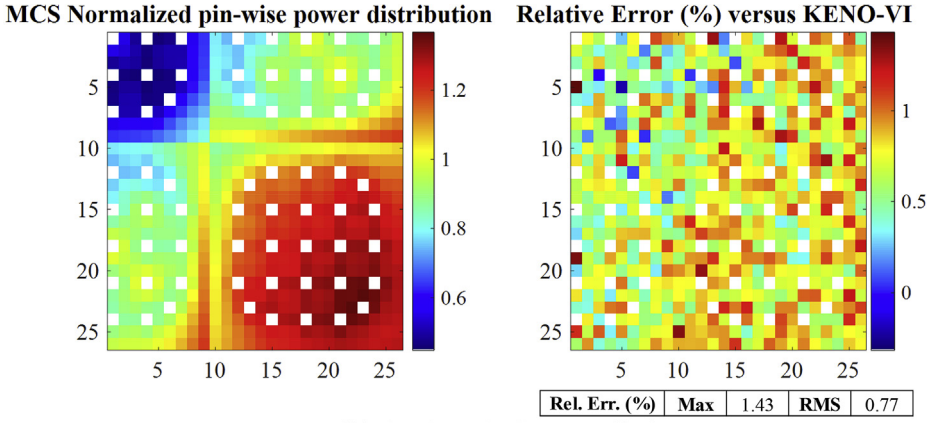

(b) 4B-2D: AIC controlled

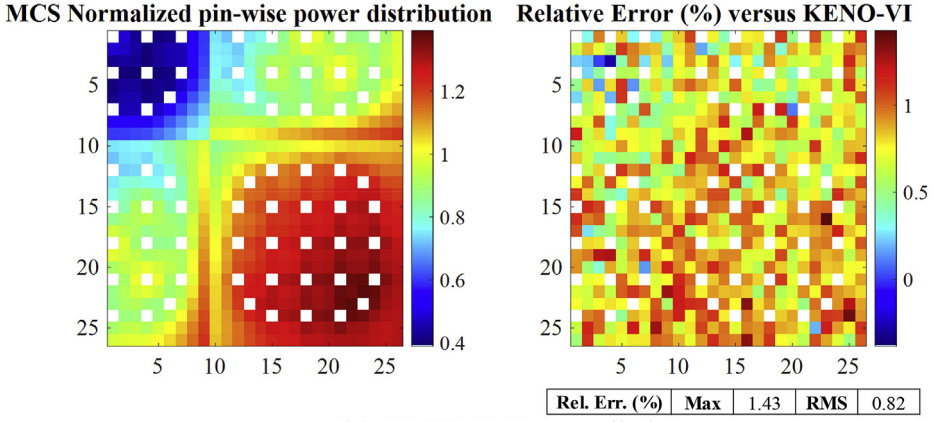

(c) 4C-2D: B_4C controlled

Fig. 8. Problem 4-2D: Pin-wise power distribution and relative error (%), MCS versus KENO-VI.

obtained between MCS and the measured data, and also between the two MC codes. Bank D DRW and IRW were also obtained by MCS and compared with the KENO-VI results as illustrated in Fig. 13. The DRW and IRW relative discrepancies vary predominantly in the range of −2 to 5% for both cases; an exception to this is the case of 90% Band D withdrawal due to the small worth.

Furthermore, the whole-core simulation case 1 (with a boron concentration of 1285 ppm and a bank D position of 167 steps withdrawn) was re-computed with a higher number of histories (750 million in total) to tally power profiles. The deviations in MCS radial and axial power profiles are correspondingly less than 0.5% and 0.8%. The normalized power distributions (normalized such that the average power equals 1.0 over the active core region) are compared with the results from KENO-VI in Fig. 14. The normalized assembly-wise radial and axial power distributions have relative differences of less than 0.7% and 1.5%, respectively. In addition, Fig. 15 depicts the average normalized pin-wise radial quarter-core power distributions obtained from MCS. The maximum deviation of the pin power is less than 1% to confirm the adequate convergence of the MCS solutions. A comparison of pin-wise power with KENO-VI was also made and shown in Fig. 16. The relative difference between MCS and KENO-VI pin power ranged from −1.35 to 2.50%. However, more than 97% of the relative difference lied between −1.0 and 1.0%, giving the RMS difference equal to

Table 11
Problem 4: Results for control rod worth (at one standard deviation).

RCCA % Withdrawn	MCS			Difference		
	k_{eff} [±3 pcm]	DRW [±4 pcm]	IRW [±4 pcm]	k_{eff} [±3 pcm]	DRW [%]	IRW [%]
257.9 cm	0.99875	–	−238	−23	–	−0.8 ± 1.9
0	0.97207	−142	−2986	−34	5.8 ± 3.2	0.4 ± 0.1
10	0.97341	−586	−2844	−27	−1.8 ± 0.8	0.1 ± 0.2
20	0.97899	−805	−2259	−37	1.4 ± 0.6	0.6 ± 0.2
30	0.98677	−536	−1454	−28	−0.9 ± 0.8	0.2 ± 0.3
40	0.99202	−351	−918	−33	2.1 ± 1.3	0.9 ± 0.5
50	0.99548	−224	−567	−26	−2.5 ± 2.0	0.1 ± 0.8
60	0.99771	−159	−342	−32	4.2 ± 2.8	1.9 ± 1.3
70	0.99930	−101	−183	−25	−1.9 ± 4.4	0.0 ± 2.4
80	1.00031	−60	−82	−27	3.3 ± 7.5	2.4 ± 5.5
90	1.00091	−22	−22	−26	−0.2 ± 20.4	−0.2 ± 20.4
100	1.00113	–	0	−25	–	–

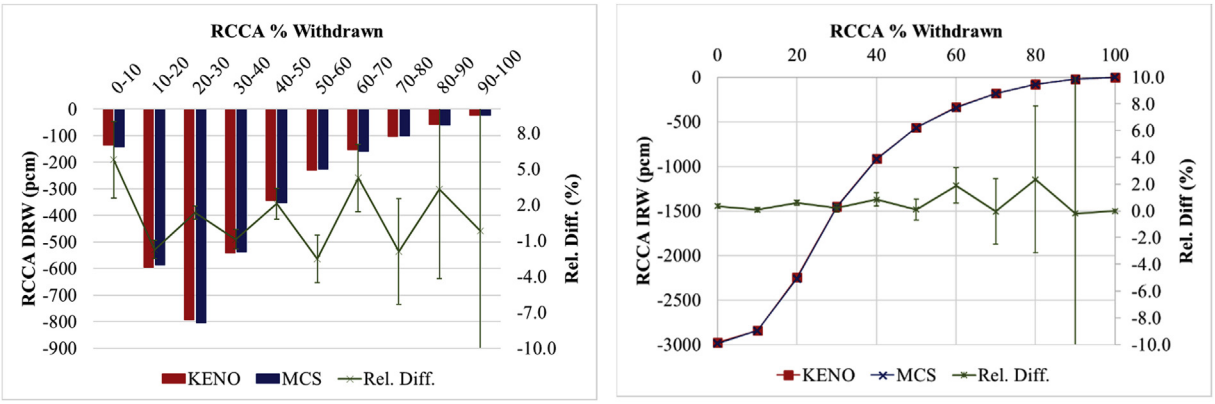

Fig. 9. Problem 4: RCCA differential rod worth (left) and integral rod worth curve (right).

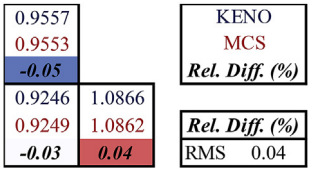

Fig. 10. Problem 4: Normalized assembly-wise radial power distribution for an octant geometry.

approximately 0.43%. Overall, the MCS power profile solutions are in great agreement with the KENO-VI reference solutions.

5. Conclusions

In this paper, the benchmark solutions of VERA problems using the UNIST MC code MCS are presented. The study consists of code-to-code comparison with KENO-VI and Serpent 2, and validation with measured data. From a simple 2D pin cell to a complicated 3D whole-core simulation, results from the MCS code are in good agreement with the reference results. Results show that numerical

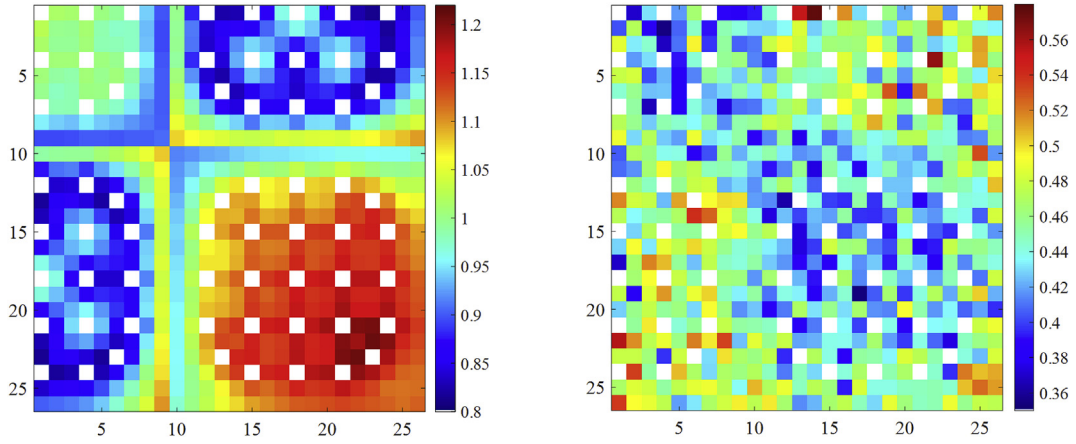

Fig. 11. Problem 4: Normalized pin-wise radial power distribution (left) and relative statistical uncertainties (right, in %) for a quarter geometry.

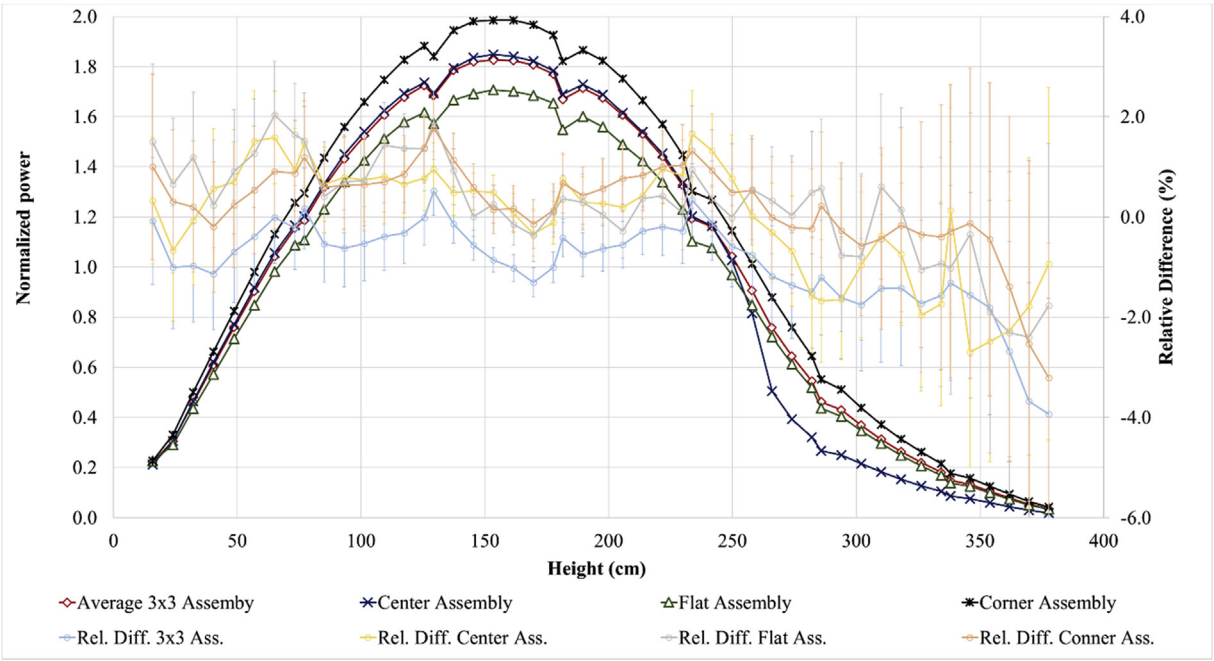

Fig. 12. Problem 4: Normalized average axial power distribution for 3 × 3 assembly lattice.

Table 12
Problem 5: Average execution time of each code.

Code	Library	Histories	# processes	Execution time (min)
MCS	ENDF/B-VII.0	3.0E+08	25	155
KENO-VI	ENDF/B-VII.0	7.5E+09	300	2640

solutions using MCS are more consistent with those of Serpent 2 than with those of KENO-VI, because MCS and Serpent 2 simulations (problems 1 to 3) are controlled to be the same. With the more complicated problems 4 and 5, MCS solutions are only compared with KENO-VI solutions. The average difference in

Table 13
Problem 5: k_{eff} results for criticality problems (at one standard deviation).

Case	RCCA Positions		k_{eff} (±4 pcm)	Difference with KENO-VI (±4 pcm)
	Bank D Withdrawn Steps	RCCA Insertion		
1	167	–	0.99972	−18
2	230	–	1.00008	−24
3	97	Bank A	0.99861	−19
4	113	Bank B	0.99892	−44
5	119	Bank C	0.99879	−25
6	18	–	0.99884	−24
7	69	Bank SA	0.99874	−28
8	134	Bank SB	0.99909	−23
9	71	Bank SC	0.99924	25
10	71	Bank SD	0.99931	34

Table 14
Problem 5: Solutions for ZPPT (at one standard deviation).

Test Result	MCS	Measured [2]	Difference with measured data	KENO-VI	Difference with KENO-VI
Initial criticality	1.00000 ±0.00003	1.00000	0 ± 3 pcm	1.00007 ±0.00001	−7±4 pcm
Rod worth (pcm)					
- Bank A	888 ± 7	843	5.3 ± 0.8%	898 ± 2	−1.2 ± 0.9%
- Bank B	875 ± 7	879	−0.5 ± 0.8%	875 ± 2	0.0 ± 0.9%
- Bank C	988 ± 7	951	3.9 ± 0.7%	984 ± 2	0.4 ± 0.8%
- Bank D	1380 ± 7	1342	2.8 ± 0.5%	1386 ± 2	−0.4 ± 0.6%
- Bank SA	453 ± 7	435	4.1 ± 1.6%	447 ± 2	1.3 ± 1.7%
- Bank SB	1056 ± 7	1056	0.0 ± 0.6%	1066 ± 2	−1.0 ± 0.7%
- Bank SC	459 ± 7	480	−4.5 ± 1.5%	499 ± 2	−8.1 ± 1.6%
- Bank SD	459 ± 7	480	−4.5 ± 1.6%	499 ± 2	−8.1 ± 1.7%
- Total	6543 ± 20	6467	1.2 ± 0.3%	6654 ± 4	−1.5 ± 0.3%
DBW (pcm/ppm)	−10.19 ± 0.06	−10.77	0.58 ± 0.06	−10.21 ± 0.02	0.02 ± 0.06
ITC (pcm/°F)	−3.48 ± 0.20	−2.17	−1.31 ± 0.20	−3.18 ± 0.04	−0.30 ± 0.20

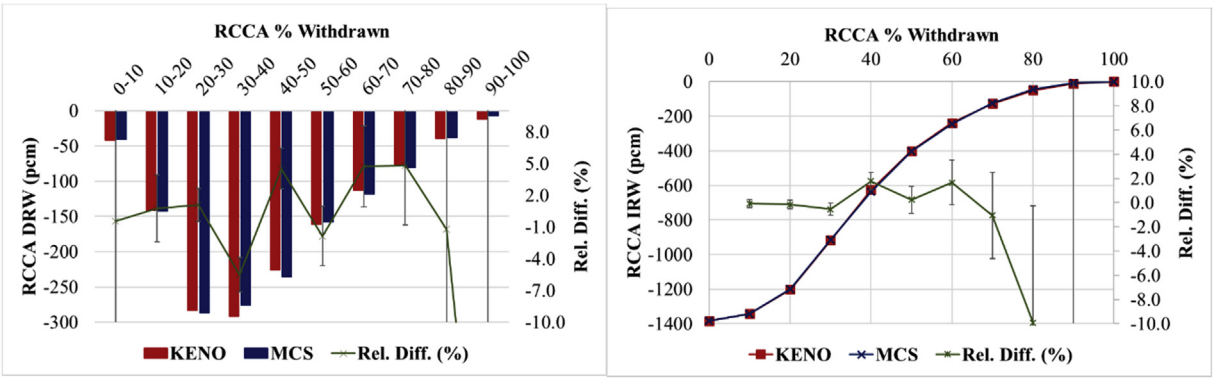

Fig. 13. Problem 5: Bank D differential rod worth (left) and integral rod worth curve (right).

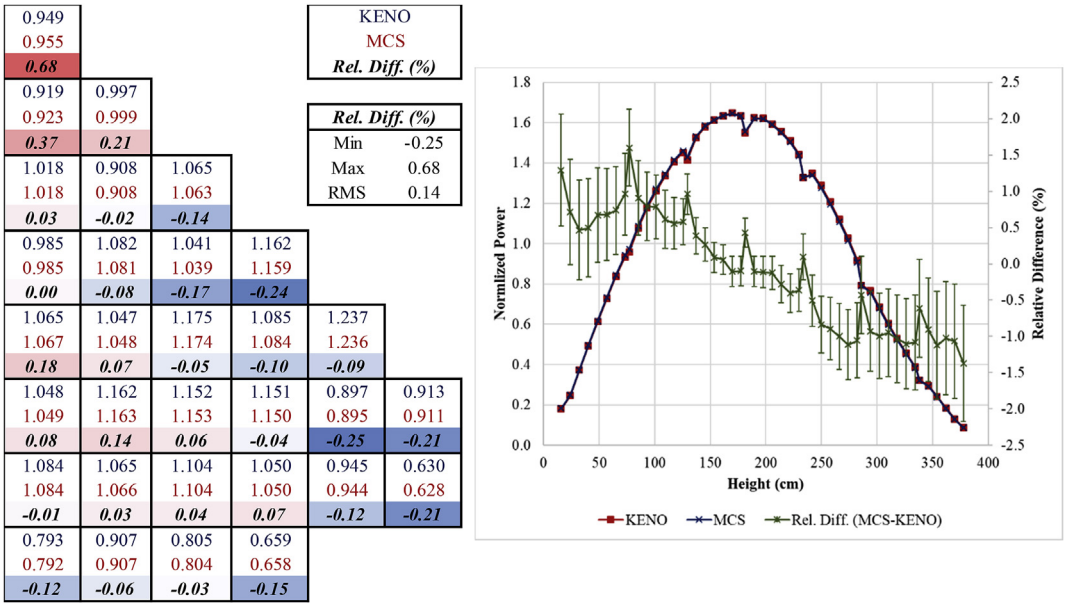

Fig. 14. Problem 5: Normalized power distribution: assembly-wise radial power for octant symmetric core (left) and average axial power for whole core (right).

eigenvalue between those MC code predictions is 26 pcm. The RMS difference in radial assembly-wise and pin-wise power profiles is less than 0.15% and 0.43%, respectively, and the bias in axial power distribution is less than 1.5%. Furthermore, the ZPPT results including the control rod worth, ITC, and DBW are also matched by MCS. In comparisons with KENO-VI and measured data, excellent agreements between MCS and KENO-VI and between MCS and measured data are obtained with the largest differences in rod

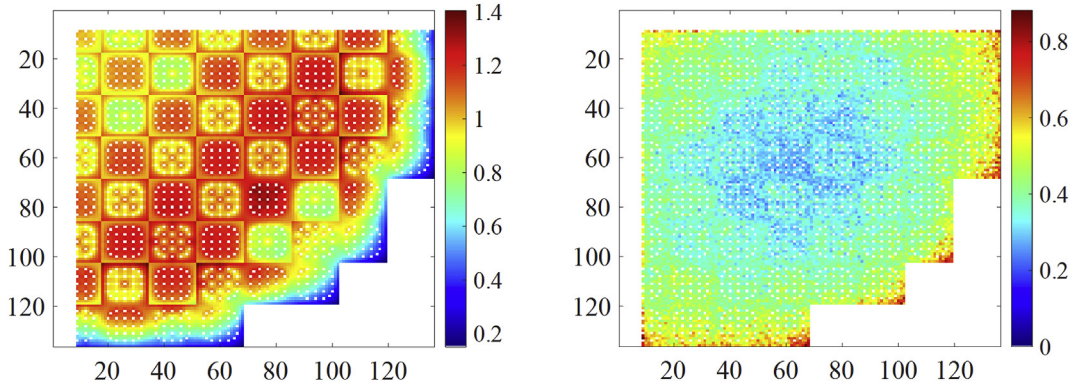

Fig. 15. Problem 5: MCS Normalized pin-wise radial power distribution for a quarter symmetric core (left) and relative standard deviation (right, in %).

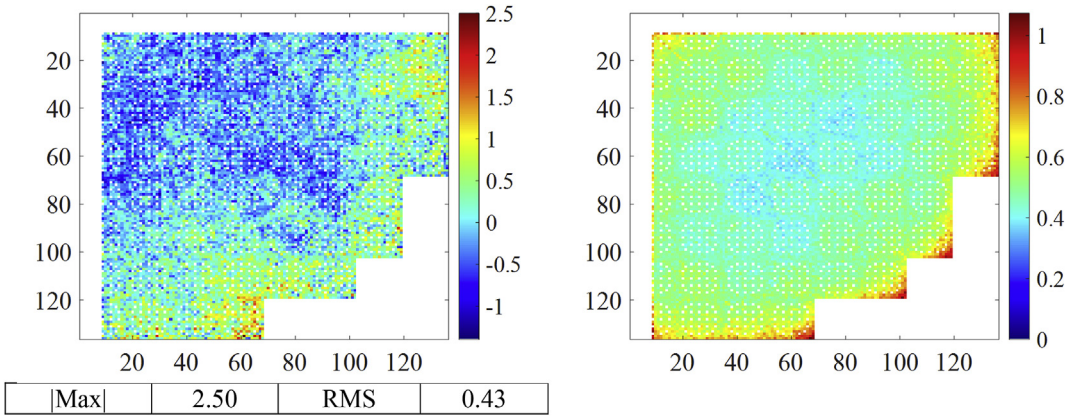

Fig. 16. Problem 5: Pin-wise radial power relative difference (left, in %) and relative standard deviation (right, in %), MCS versus KENO-VI.

worth being 8.1% and 5.3%, respectively. In addition, good agreements in ITC and soluble boron worth are observed between MCS and measured data, and also between the two MC codes.

In conclusion, the use of MCS as a simulation tool for whole-core analysis in predicting the eigenvalue, detail pin power distribution, control rod worth, and reactivity coefficients has been successfully demonstrated. However, a limitation of this study is that it only focuses on the steady state of the reactor without thermal-hydraulic feedback. Therefore, the MCS simulation of a single assembly and whole core coupled with the internal thermal-hydraulic feedback module and multi-physics multi-cycle depletion calculations for WBN1 will be presented in a separate research paper.

Acknowledgments

This work was supported by the National Research Foundation of Korea (NRF) grant funded by the Korean government's Ministry of Science and Information and Communications Technology (MSIT) (No. NRF-2019M2D2A1A03058371).

Appendix A. Supplementary data

Supplementary data to this article can be found online at https://doi.org/10.1016/j.net.2019.10.023.

References

[1] The Consortium for advanced simulation of Light water reactors (CASL). http://www.casl.gov, 2014.
[2] A.T. Godfrey, VERA Core Physics Benchmark Progression Problem Specifications, Consortium for Advanced Simulation of LWRs, 2014. CASL-U-2012-0131-004.
[3] T.J. Labossiere-Hickman, B. Forget, Selected VERA core physics benchmarks in OpenMC, in: 2017 ANS Winter Meeting and Nuclear Technology Expo, Washington, DC, USA, Oct 29 – Nov 2, 2017.
[4] Z. Luo, J. Guo, G. Yu, K. Wang, S. Liu, Solutions to VERA core physics benchmark progression problems 1 to 6 based on RMC, in: 2017 ANS Winter Meeting and Nuclear Technology Expo, Washington, DC, USA, Oct 29 – Nov 2, 2017.
[5] H. Lee, W. Kim, P. Zhang, A. Khassenov, Y. Jo, D. Lee, Development status of Monte Carlo code at UNIST, in: Proceedings of the Korean Nuclear Society Spring Meeting, Jeju, Korean Nuclear Society, May 11-13, 2016 [USB].
[6] H. Lee, C. Kong, D. Lee, Status of Monte Carlo code development at UNIST, in: Proceedings of the PHYSOR Conference, Kyoto, Japan Atomic Energy Agency, Sep 28 – Oct 3, 2014 [USB].
[7] J. Jang, W. Kim, S. Jeong, E. Jeong, J. Park, M. Lemaire, H. Lee, Y. Jo, P. Zhang, D. Lee, Validation of UNIST Monte Carlo code MCS for criticality safety analysis of PWR spent fuel pool and storage cask, Ann. Nucl. Energy 114 (2018) 495–509.
[8] H. Lee, W. Kim, P. Zhang, A. Khassenov, J. Park, J. Yu, S. Choi, H. Lee, D. Lee, Preliminary simulation results of BEAVRS three-dimensional Cycle 1 whole core depletion by UNIST Monte Carlo code MCS, in: Proceedings of the Mathematics and Computations (M&C) Conference, Jeju, Korean Nuclear Society, Apr 16-20, 2017 [USB].
[9] H. Lee, E. Jeong, H. Lee, H.C. Lee, D. Lee, Verification of MCS VHTR modeling capability, in: Proceedings of the RPHA17 Conference, Chengdu, Nuclear Power Institute of China, Aug 24-25, 2017 [USB].
[10] T.D.C. Nguyen, H. Lee, J. Choe, H.C. Shin, H.S. Lee, D. Lee, Low power physics test analysis of APR1400 reactor core by UNIST Monte Carlo code MCS, in: Proceedings of the RPHA17 Conference, Chengdu, Nuclear Power Institute of China, Aug 24-25, 2017 [USB].
[11] V. Dos, H. Lee, Y. Jo, M. Lemaire, C.J. Park, D. Lee, Verification of MCS Monte Carlo code for the JRTR research reactor, in: Proceedings of the PHYSOR Conference, Cancun: American Nuclear Society, Apr 22-26, 2018 [USB].
[12] J. Jang, J. Choe, S. Choi, H. Lee, B. Ebiwonjumi, H.C. Shin, D. Lee, Boron-free SMPWR analysis with MCS and STREAM codes, in: Proceedings of the RPHA17 Conference, Chengdu, Nuclear Power Institute of China, Aug 24-25, 2017 [USB].
[13] T.D.C. Nguyen, H. Lee, J. Choe, M. Lemaire, D. Lee, APR-1400 whole-core depletion analysis with MCS, in: Proceeding of M&C 2019 Conference, Oregon USA, August 25-29, 2019 [USB].
[14] V. Dos, H. Lee, X. Du, D. Lee, MCS analysis of 1000MWth sodium-cooled fast reactor, in: Proceeding of ICAPP Conference, France, May 12-15, 2019 [USB].
[15] N.N.T. Mai, Y. Jo, H. Lee, A. Cherezov, D. Lee, Whole-core Monte Carlo analysis of mox-3600 core in NEA-SFR benchmark using MCS code, in: Proceeding of KNS Autumn Meeting, Yeosu, Korea, October 24-26, 2018 [USB].
[16] N.N.T. Mai, C. Kong, H. Lee, S. Choi, D. Lee, Application of MCS code for spent duel cask analysis, in: Proceeding of KNS Autumn Meeting, Yeosu, Korea, October 24-26, 2018 [USB].
[17] A.T. Godfrey, B.S. Collins, K.S. Kim, R. Montgomery, J.J. Powers, R.K. Salko, S.G. Stimpson, W.A. Wieselquist, K.T. Clarno, J.C. Gehin, S. Palmtag, VERA Benchmarking Results for Watts Bar Nuclear Plant Unit 1 Cycles 1-12, Consortium for Advanced Simulation of LWRs, 2015. CASL-U-2015-0206-000.
[18] M.E. Dunn, C.L. Bentley, S. Goluoglu, L.S. Paschal, L.M. Petrie, H.L. Dodds, Development of a continuous energy version of KENO V.a, Nucl. Technol. 119 (3) (1997) 306–313.
[19] J. Leppänen, M. Pusa, T. Viitanen, V. Valtavirta, T. Kaltiaisenaho, The Serpent Monte Carlo code: status, development and applications in 2013, Ann. Nucl. Energy 82 (2015) 142–150.